HEFAT2014
10th International Conference on Heat Transfer, Fluid Mechanics and Thermodynamics
14 – 16 July 2014
Orlando, Florida

STUDY OF UNSTEADY COMBUSTION PROCESSES CONTROLLED BY DETAILED CHEMICAL KINETICS

Liberman M. A.
Nordita, KTH Royal Institute of Technology and Stockholm University
Roslagstullsbacken 23, 10691 Stockholm
Sweden
E-mail: michael.liberman@nordita.org

ABSTRACT

Our understanding of the fundamentals of combustion processes to large extent was heavily based on the use of a fairly simplified one-step Arrhenius kinetics model. However, the chemical mechanisms are an important factor significantly influencing the processes. The range of validity of simplified chemical schemes is necessary very limited. Furthermore, it became clear that the use of a one-step Arrhenius model may lead to only a very basic picture describing qualitatively a few major properties of the combustion phenomena with some poor accuracy if any, often rendering misinterpretation of a verity of combustion phenomena. Moreover, many important features of combustion can not be explained without account of the reactions chain nature. An accurate description of unsteady, transient combustion processes controlled by chemical kinetics requires knowledge of the detailed reaction mechanisms for correct reproducing combustion parameters in a wide range of pressures and temperatures. The availability of such models is essential for gaining scientific insight into the most fundamental combustion phenomena and it is an essential factor for design of efficient and reliable engines and for controlling emissions. In this lecture we consider the option of a reliable reduced chemical kinetic model for the proper understanding and interpretation of the unsteady combustion processes using hydrogen-oxygen combustion as a quintessential example of chain mechanisms in chemical kinetics. Specific topics covered several of the most fundamental combustion phenomena including: the regimes of combustion wave initiated by initial temperature non-uniformity; ignition of combustion regimes by the localized transient energy deposition; the spontaneous flame acceleration in tubes with no-slip walls; and the transition from slow combustion to detonation.

INTRODUCTION

An accurate knowledge of the detailed reaction mechanisms is of paramount importance for understanding and correct description of kinetically controlled unsteady combustion processes such as ignition and self-ignition processes (e.g. engine knock), flame acceleration and extinction, the deflagration to detonation transition (DDT), etc. Development and exploitation of reliable detailed chemical kinetic models, identification of the important kinetic pathways and accurate kinetic–transport models remain among the major challenges in combustion science and technology being essential for the design of efficient and reliable engines and for controlling emissions. Nowadays, computational fluid dynamics became one of the main tools in design of advanced combustors, especially in the developing stage where experiments are rather expensive and resource consuming. From the beginning our understanding of key combustion phenomena was essentially based on a one-step Arrhenius kinetics model. While a one-step Arrhenius kinetics model in many cases makes possible to solve the problem in question in explicit analytical form, many important features of combustion can not be explained without account of the reactions chain nature. The range of validity of simplified schemes is necessary very limited and their applicability to the understanding and modeling of combustion phenomena must be examined with great care. Furthermore, it became clear that the use of a one-step Arrhenius model has not always been interpreted properly, rendering misinterpretation of a verity of combustion phenomena. A one-step Arrhenius kinetics model does not reproduce even

two distinct stages of the combustion reaction: induction stage and exothermal one. Another fundamental difference between a one-step Arrhenius model and the chain-branching reaction is an avalanche multiplication of intermediate species, atoms and radicals, and their repetitive reactions constituting reaction chains. In principle, the detailed reaction mechanisms were developed for different combustible mixtures and today are available and can be used in the simulation of spatially homogeneous reaction systems. If, however, real three-dimensional and often turbulent flows are considered, we have to use reduced chemical schemes, since the use of detailed reaction mechanisms involves massive computing times which can be difficult and even impossible to implement. Even in the combustion of simple hydrocarbons, the chemical kinetics is reproduced by relatively large reaction mechanisms, and for complex hydrocarbons the number of chemical species can be up to several hundreds and the number of elementary reactions up to several thousands. It is known [1, 2] that in many cases both quantitative and qualitative features of the studying processes essentially depend on the choice of chemical kinetics model. Therefore, there is great interest in reduced reliable chemical reaction schemes consisting of not too large number of elementary reactions.

A quintessential example of chain mechanisms in chemical kinetics and combustion science is the H_2-O_2 mechanism, which has been a major topic of research for many decades. The number of available mechanisms are significant, yet there are uncertainties related to the elementary reactions involved [3] and available for validation experimental data is scarce, especially for low-temperature kinetics ($T<1000K$), which is particularly important for the understanding of ignition. A little or uncertain data are available for the elementary reactions and a laminar flame speed at elevated pressure ranges. To reproduce transient processes, which are accompanied by compression and shock waves, it is necessary to take into account parameters such as induction period and period of exothermal reaction, which determine the chemical time scales competing with transport time scales in establishing the zone of energy release, which in turn determines the evolution of the flame. Even more important for a correct description of transient processes is the pressure dependence of flame parameters. It is important to get the solution of basic problems using a model which validation is similar to that used in the simulation of multidimensional unsteady problems. Here we consider different widely used kinetic schemes for H_2/O_2 and H_2-air mixtures using the gas-dynamics transport model for laminar flame characteristics and taking into account the correlations between evolutionary and gas-dynamics parameters at different initial pressures. We then consider some fundamental unsteady combustion problems, which understanding and solution require to use detailed chemical kinetic schemes.

REDUCED CHEMICAL KINETIC MODELS

The standard procedure for verification of the reduced chemical schemes is the numerical solutions of the 0D problem and the validation procedures consisting of the experimental databases containing data on induction periods, equilibrium temperature, and composition of the combustion products. The method of solution of 1D eigenvalue problems often used for calculation of the laminar flame speed is far distinct mathematically from the computational gas-dynamics setups used for simulation of multidimensional transient processes and from experimental setups of the ignition and combustion and in some cases it may cause considerable differences between experimental and numerically obtained data. On the other hand in order to simulate an unsteady problem it is necessary to validate the codes and the models using the same mathematical methods and models which are used for the modeling of combustion phenomena.

Usually the verification of the reduced kinetic schemes covers the data on induction periods, equilibrium composition and temperature of the products. The latter are defined by the thermodynamic equilibrium laws and are pure thermodynamic characteristics and as a rule they are in a good agreement with experimental data. The only evolutionary parameter is the induction period, which determines duration of the endothermal stage in reaction. In some cases the exothermal stage duration may be principal as the scales of energy release may determine the gas-dynamics flows. To reproduce transient processes, such as e.g. flame acceleration, ignition, which are accompanied by compression and shock waves, it is necessary to take into account correlations between evolutionary parameters (induction period and duration of exothermal stage) and gasdynamics parameters (laminar flame speed and its thickness), which determine the chemical time scales competing with transport time scales in establishing the zone of energy release and stipulating the flame evolution.

We consider here some widely used chemical kinetic schemes for hydrogen-air and hydrogen-oxygen [4-9] using the full gas dynamics models with standard transport model [10] for laminar flame characteristics. The governing equations used for

evaluation of kinetic schemes are the one-dimensional time-dependent, reactive Navier-Stokes equations including the effects of compressibility, molecular diffusion, thermal conduction, viscosity and chemical kinetics for the reactive species with subsequent chain branching, production of radicals and energy release.

$$\frac{\partial \rho}{\partial t}+\frac{\partial(\rho u)}{\partial x}=0 \qquad (1)$$

$$\frac{\partial Y_i}{\partial t}+u\frac{\partial Y_i}{\partial x}=\frac{1}{\rho}\frac{\partial}{\partial x}\left(\rho D_i\frac{\partial Y_i}{\partial x}\right)+\left(\frac{\partial Y_i}{\partial t}\right)_{ch} \qquad (2)$$

$$\rho\left(\frac{\partial u}{\partial t}+u\frac{\partial u}{\partial x}\right)=-\frac{\partial P}{\partial x}+\frac{\partial \sigma_{xx}}{\partial x}, \qquad (3)$$

$$\rho\left(\frac{\partial E}{\partial t}+u\frac{\partial E}{\partial x}\right)=-\frac{\partial(Pu)}{\partial x}+\frac{\partial}{\partial x}(\sigma_{xx}u)+$$
$$\frac{\partial}{\partial x}\left(\kappa(T)\frac{\partial T}{\partial x}\right)+$$
$$\sum_k\frac{h_k}{m_k}\left(\frac{\partial}{\partial x}\left(\rho D_k(T)\frac{\partial Y_k}{\partial x}\right)\right) \qquad (4)$$

$$P=\left(\sum_i\frac{R_B}{m_i}Y_i\right)\rho T=\rho T\sum_i R_i Y_i, \qquad (5)$$

$$\varepsilon=c_v T+\sum_k h_k Y_k, \qquad (6)$$

$$\sigma_{xx}=\frac{4}{3}\mu\left(\frac{\partial u}{\partial x}\right) \qquad (7)$$

Concentrations $Y_i=\rho_i/\rho$ of the species (H_2, H, O_2, O, H_2O, OH, HO_2, H_2O_2, M (N, N_2, NO, NO_2, Ar), are defined by the equations of chemical kinetics, which is solved with the aid of Gear method [11]

$$\frac{dY_i}{dt}=F_i(Y_1,Y_2,...Y_N,T),\quad i=1,2,...N. \qquad (8)$$

The number of the reactions in Eq. (8) can be from 19 to 37 depending on the chemical scheme, where the right hand parts of Eq. (8) contain the rates of chemical reactions, which depend on temperature according to the Arrhenius law in a standard form [6]. Here we use the standard notations: P, ρ, u, are pressure, mass density, and flow velocity, $E=\varepsilon+u^2/2$ is the total energy density, ε is the inner energy density, R_B - is the universal gas constant, m_i - the molar mass of i-species, $R_i=R_B/m_i$, n is the molar density, σ_{ij} is the viscous stress tensor, $c_v=\sum c_{vi}Y_i$ is the constant volume specific heat, c_{vi} - the constant volume specific heat of i-species, h_i - the enthalpy of formation of i-species, $\kappa(T)$ and $\mu(T)$ are the coefficients of thermal conductivity and viscosity, $D_i(T)$ - is the diffusion coefficients of i-species. The equations of state for the reactive mixture and for the combustion products were taken with the temperature dependence of the specific heats and enthalpies of each species borrowed from the JANAF tables and interpolated by the fifth-order polynomials. The viscosity, thermal conductivity and diffusivity coefficients of the mixture were calculated from the gas kinetic theory using the Lennard-Jones potential [10]. The system of gas dynamics equations is solved using Lagrange-Euler method [12], which was modified and improved for solving 2D and 3D problems with a detailed chemical kinetic schemes (see e.g. [13]).

The calculated induction periods and exothermal stage durations dependencies on initial temperature for the stoichiometric hydrogen-air mixture at 1atm, using chemical schemes [4-9], are shown in Fig.1 together with available experimental data. Almost linear curves intersecting the induction period dependencies represent an exothermal stage duration which determines the time scale of energy release inside the reaction zone. Though there are differences within (10-15)% in the induction time at low temperatures, it may be not essential if the endothermic induction time is larger than characteristic gas-dynamics time of the problem.

The calculated laminar flame speeds U_f at normal pressure 1atm in stoichiometric hydrogen-air mixture for different equivalent ratio of hydrogen-air mixture are presented in Fig. 2.

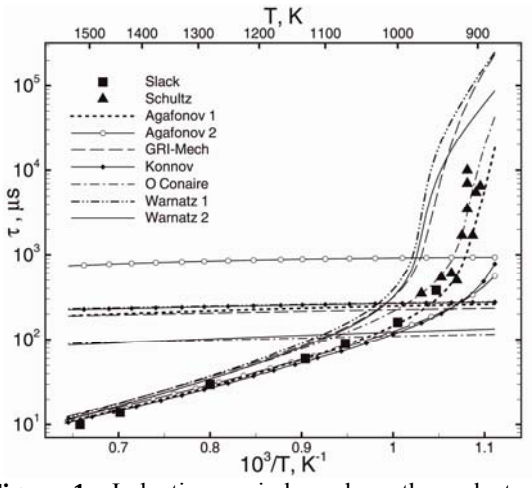

Figure 1 Induction periods and exothermal stage durations dependencies on initial temperature of stoichiometric H_2-air mixture at 1atm.

The differences in the induction time given by different schemes at low temperatures cause more essential difference for the induction time calculated

at elevated pressures shown in Fig. 3(a, b, c), and there is considerable difference of the calculated values of induction from the experimental data in the low temperature region at pressure greater then 2.5atm when three-body collisions become essential.

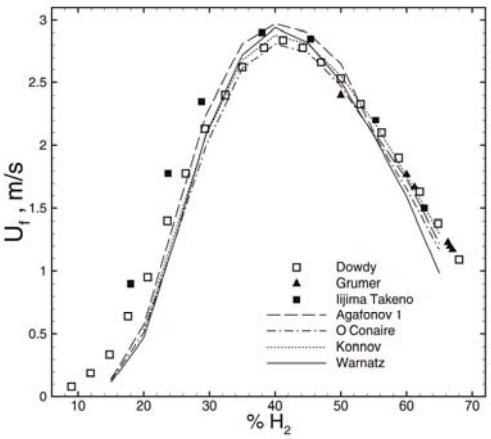

Figure 2 Laminar flame speed dependence on the volume fraction of H_2 for H_2-air mixture.

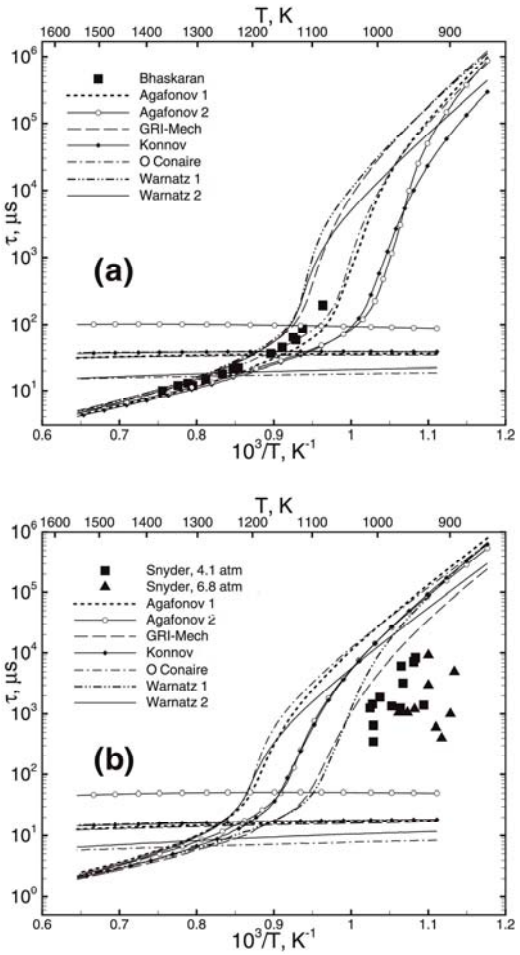

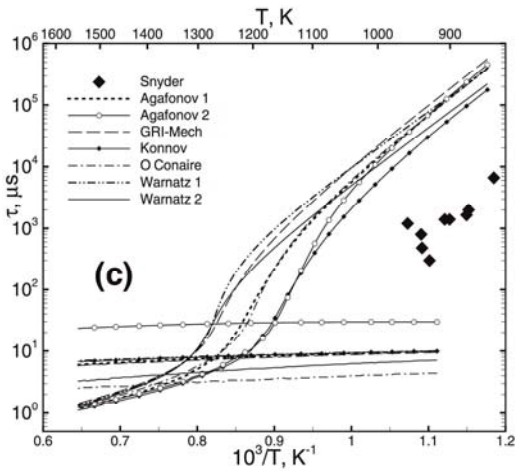

Figure 3(a, b, c) Induction periods and exothermal stage durations dependencies on initial temperature of stoichiometric hydrogen-air mixture (a)- 2.5atm; (b) - 5.0atm; (c) - 8.8atm.

The velocity-pressure dependence calculated for different kinetic schemes, experimental data and analytical velocity-pressure dependence for hydrogen-oxygen approximated [14] as $U_f \propto P^{(n-2)/2}$ for overall reaction order 2.74 (dotted line) [15, 16] are shown in Fig.4. The experimental data are quite distinct from the calculations and from each other and the distinctions rise with the pressure. The difference in time scales and corresponding difference in flame width calculated using different kinetic schemes for highly reactive hydrogen-oxygen become more noticeable. The main difference in the induction time given by different schemes is in the region of low temperatures.

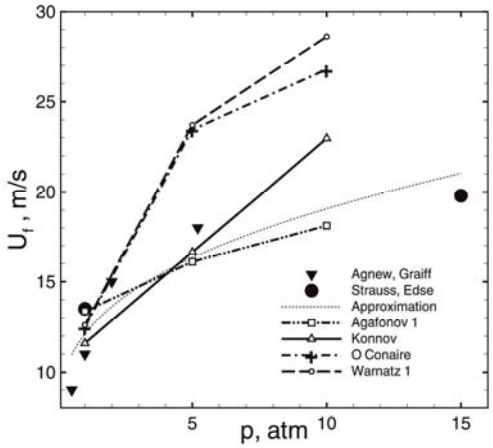

Figure 4 Speed-pressure dependence of laminar flame in H_2/O_2 mixture.

Thus, further improvement and the development of low-temperature kinetics (T<1000K) is particularly significant for the understanding of the ignition and self-ignition processes. While speed of sound and therefore characteristic hydrodynamic time scales do not depend on pressure, the induction time, especially at the temperature range (1000÷1200)K is considerably sensitive to pressure. This and the different pressure dependencies given by different reduced schemes must be taken into account with a great care while modeling unsteady combustion processes.

COMBUSTION REGIMES INITIATED BY INITIAL TEMPERATURE NONUNIFORMITY

In most practical cases ignition arises from a small area of combustible mixture, which is locally heated by means of electric spark, hot wire, focused laser light and the like. Such local energy release results in the formation of the initial nonuniform distribution of temperature and concentration of reagents which determines further evolution of the reaction wave depending on the mixture reactivity and the initial pressure. The initiation or ignition of the chemical reaction wave is one of the most fundamental problems in combustion physics. One needs to know how combustion starts and how initial conditions influence the regime of reaction wave which propagates out from the ignition location. What type of combustion wave is formed depending on the ignition conditions?

For the first time regimes of chemical reaction wave ignited by the initial nonuniform temperature distribution have been studied by Ya. B. Zeldovich [17], who introduced the concept of *spontaneous reaction wave*. The basic idea was that the reaction is ignited at the point of minimum induction time and correspondingly maximum temperature and then spreads along the gradient at neighboring locations where τ_{ind} is longer with velocity

$$U_{sp} = \left|\left(d\tau_{ind}/dx\right)\right|^{-1} = \\ = \left|\left(\partial\tau_{ind}/\partial T\right)^{-1}\left(\partial T/\partial x\right)^{-1}\right| \qquad (9)$$

For a one-step chemical reaction model the induction time, τ_{ind}, is defined as a time-scale of the maximum reaction rate. In the case of real chain branching chemistry this is the time scale for the stage of endothermic chain initiation and branching reactions. The value of U_{sp} depends only on the gradient steepness and does not depend on thermal conduction or sound speed. The Zeldovich's concept of the spontaneous reaction wave opened an avenue to study scenario of the reaction ignition and the evolution of spontaneous wave initiated by the initial non-uniformity in temperature or reactivity in different regimes of combustion wave and therefore of great fundamental and practical importance.

In the subsequent studies researchers have employed a one-step Arrhenius model, and the studies have been focused mainly on the regime of direct ignition of a detonation by the initial temperature gradient discovered by Zeldovich and co-authors [18]. All the same the models with a simplified one-step chemical kinetics may lead only to only poor accuracy if any, sometime giving even qualitatively incorrect interpretation. Subsequently it was shown using two-step and three-step models, which to some extent mimic the chain-branching kinetics with a simplified notional reaction scheme between a set of pseudo-species, that the one-step chemical model does not properly describe systems governed by chain-branching reaction, and the one-step model is not appropriate for simulating detonation initiation in systems governed by chain-branching reactions.

We consider regimes of chemical reaction wave in hydrogen-oxygen initiated be the initial temperature gradient depending on the steepness of the gradient and using a detailed chemical kinetic model [19, 20]. The initial conditions are quiescent and uniform mixture apart from a linear gradient in temperature (and hence density), with the left boundary at $x = 0$ being a solid reflecting wall, where $u(0,t) = 0$:

$$T(x,0) = T^* - (T^* - T_0)(x/L),\ 0 \le x \le L \qquad (10)$$

$$P(x,0) = P_0,\ u(x,0) = 0. \qquad (11)$$

The initial temperature gradient is characterized by the temperature, $T(0,0) = T^*$, at the top left edge, by the mixture temperature, $T(x > L, 0) = T_0$, outside the gradient and by the gradient steepness, $(T^*-T_0)/L$. The "gradient scale", L, characterizes the gradient steepness for the fixed value of (T^*-T_0) and can be viewed as the size of the initial temperature gradient. The governing equations are the one-dimensional, multispecies reactive Navier-Stokes equations (1-8). In what follows we consider the temperature gradients of different steepness at the initial pressure 1atm with T*=1500K, T_0=300K.

Fig. 5(a) shows evolution of the spontaneous reaction wave and the pressure waves velocities for $L = 8\text{cm}$, $T^* = 1500\,\text{K}$. The corresponding evolution of the temperature and the pressure profiles is shown in Fig. 5(b). The velocity of spontaneous wave initiated by the initial temperature gradient decreases as the wave propagates along the gradient. It reaches the minimum value at the point close to the cross-over temperature where it is caught-up with the pressure wave, which was generated behind the

spontaneous wave. After the intersection of the spontaneous wave and the pressure wave, the spontaneous wave transforms into combustion wave and the pressure wave steepens into the shock wave. For a shallow enough gradient, such that the minimum speed of spontaneous wave is of the order of the sound speed at the top of the gradient, the intensity of the shock wave formed ahead of the reaction wave is sufficient to accelerate the reaction in the flow behind the shock. The pressure peak formed at the reaction front grows at the expense of energy released in the reaction and the result of the positive feedback is a detonation wave.

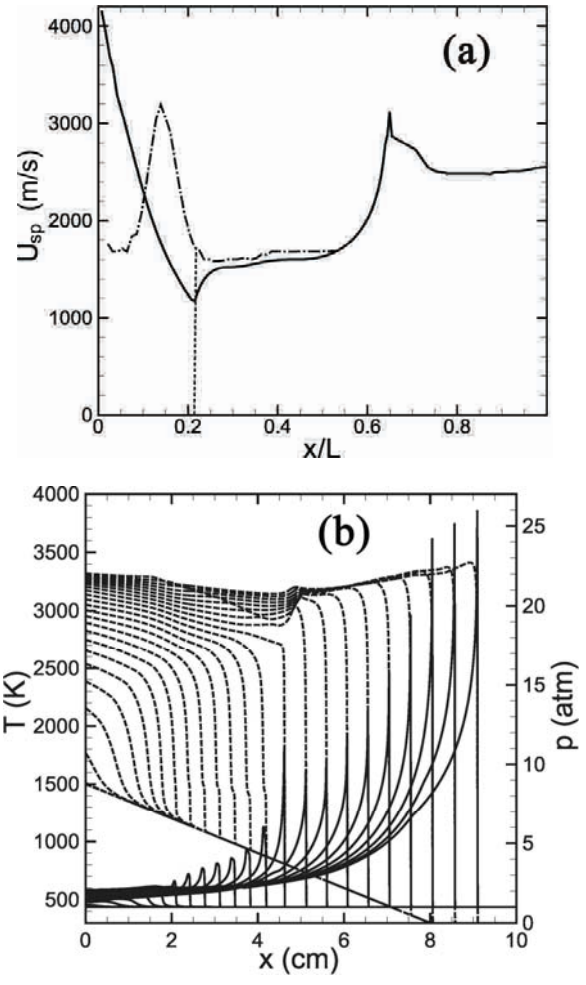

Figure 5(a, b) (a): Velocities of the spontaneous wave (solid lines) and pressure wave (dash-dotted lines) computed for the temperature gradient L=8cm, T*=1500K in H_2-O_2 mixture, P_0=1atm. (b): Evolution of the temperature (dashed lines) and pressure (solid lines) profiles (intervals 2μs) during the detonation formation.

For a steeper temperature gradient (L=7cm) the velocity of spontaneous wave in the minimum point is not sufficient to sustain synchronous amplification of the pressure pulse. As a result, the pressure wave runs ahead of the reaction wave, the velocity of the reaction wave decreases, and the resulting regime is a deflagration wave. Fig. 6(a) shows evolution of the reaction and the pressure waves velocities for $L = 7\text{cm}$, $T^* = 1500\,\text{K}$. The corresponding evolution of the temperature and the pressure profiles is shown in Fig. 6(b).

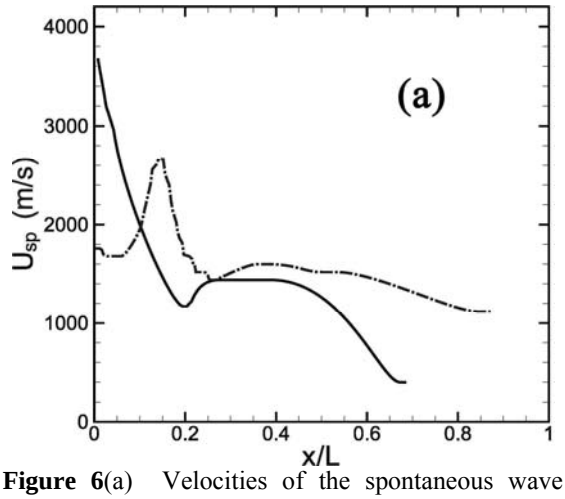

Figure 6(a) Velocities of the spontaneous wave (solid lines) and pressure wave (dash-dotted lines) computed for the temperature gradient L=7cm, T*=1500K in H_2-O_2 mixture, P_0=1atm.

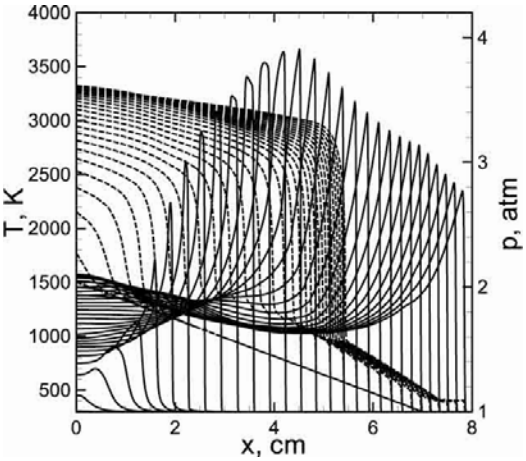

Figure 6(b) Pressure (solid lines) and temperature (dashed lines) profiles evolution for the conditions of Fig. 6(a) (Δt=2μs).

The pressure waves generated during the exothermic stage of reaction can couple and evolve into a self-sustained detonation wave, or produce a flame and a decoupled shock depending on the

gradient steepness. Possible regimes of the combustion wave inspired by the spontaneous wave initiated by the temperature gradient depend on the gradient steepness and on the ratio between the speed of spontaneous wave at the point where the spontaneous wave velocity reaches minimum and the characteristic velocities of the problem [19, 20], which are: the normal laminar flame speed, U_f, the sound speeds $a_0=a(T_0)$ and $a^*=a(T^*)$, the Neumann, a_N, and the Chapman-Jouguet, U_{CJ}, velocities. The limiting case $\nabla T \to 0$, $U_{sp} \to \infty$ corresponds to the adiabatic explosion. In another limiting case of a very steep gradient ("hot wall"), a deflagration with the normal flame velocity is ignited. The latter is bounded from below by the minimum size of the hot region, for which the rate of heat removal from the "hot wall" is larger than the normal flame velocity.

Diagram in Fig.7 shows possible combustion regimes depending on the ratio between the velocity of spontaneous wave (the gradient steepness) at the minimum point and the characteristic velocities of the problem.

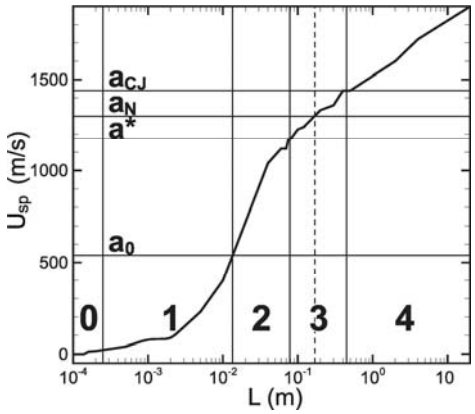

Figure 7 Regimes of the reaction waves initiated by temperature gradients of different steepness in H_2/O_2

If $U_{sp} < U_f << a_0$ (domain 0), the rate of the heat transfer by thermal conduction is greater than the spontaneous wave velocity, and the resulting regime is a deflagration wave propagating due to thermal conduction with the normal flame velocity. For $U_f < U_{sp} < a_0$ (domain 1) the pressure wave overtakes the deflagration wave, and the fast deflagration wave propagates at nearly constant slightly elevated pressure. If $a_0 < U_{sp} < a^*$, then the pressure wave overtakes the reaction wave to form a weak shock wave that compresses and heats the gas further speeding up the deflagration wave (domain 2). If $a^* < \min\{U_{sp}\} < a_N < a_{CJ}$ the reaction wave accelerates behind the shock and the transition to detonation occurs due to the formation and amplification of the pressure peak at the front of the reaction wave (domain 3). If $a_N < \min\{U_{sp}\} < a_{CJ}$ then a quasi-stationary structure consisting of a shock wave and reaction zone is formed, which transforms into a detonation propagating down the temperature gradient. If $a_{CJ} < \min\{U_{sp}\}$, the intersection of the pressure wave and the spontaneous wave creates a classical structure of a detonation wave with the reaction initiated by the leading shock (domain 4).

Scales of temperature gradients capable to ignite one or another combustion regime are considerably different (up to several orders of magnitude) for the detailed chemical model and a single-step model. First, the reaction for a one-step model is exothermic for all temperatures, while chain branching reactions begins with neutral or endothermic induction stage and therefore, the gasdynamics is effectively "switched-off" during the induction stage. On the contrary for the one-step model the spontaneous wave is essentially affected by the gas-dynamics from the very beginning, so that it is always the determining factor. Therefore, the velocity of spontaneous wave produced by the same temperature gradient is considerably smaller in the early stage for the chain-branching reaction compared with that for a one-step model. The induction time for a single-step Arrhenius model is several orders of magnitude shorter than the real one. To match more or less accurately the induction time with experimental data unrealistically high activation energy should be taken using a one-step model. As a result, the temperature gradient for initiating all possible combustion regimes is much steeper for a one-step model compared to that for a detailed chemical kinetics.

Fig. 8(a) and Fig. 8(b) show the scales of the temperature gradients calculated for the detailed chemical model of H_2/O_2 and for a one-step model.

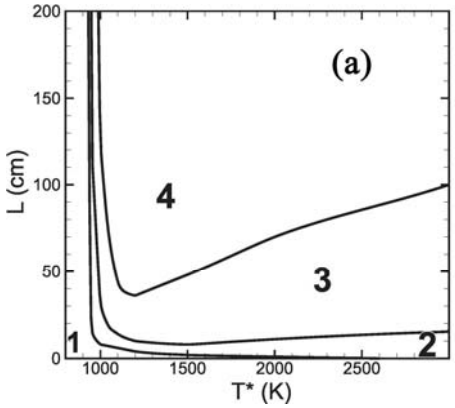

Figure 8(a) Scales (inverse steepness) of the temperature gradient in H_2/O_2 corresponding to the boundaries between regimes 1, 2, 3, 4 calculated with the detailed chemical model.

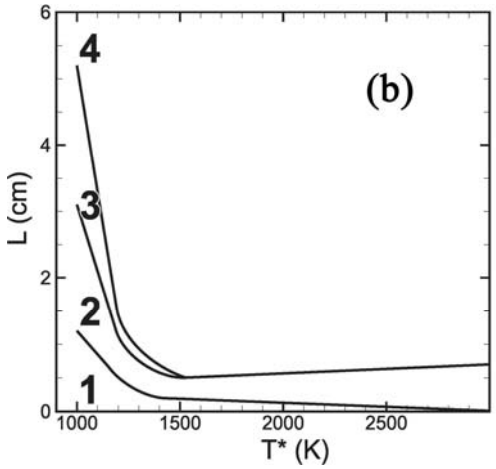

Figure 8(b**)** Scales (inverse steepness) of the temperature gradient in H_2/O_2 corresponding to the boundaries between regimes 1, 2, 3, 4 calculated for a one-step model.

The induction time increases if a combustible mixture is diluted by neutral gas and for a lower reactive mixtures. For example, in a stoichiometric hydrogen-air mixture, which can be viewed as H_2/O_2 diluted by nitrogen not involving in the chain-branching reaction, the induction time increases by 2-3 times in a wide temperature range compared to a stoichiometric hydrogen-oxygen mixture. So that the main difference between hydrogen-air compared to hydrogen-oxygen is the reduced velocity of spontaneous waves for the same temperature gradients. As a result, the scales of the temperature gradient required for initiating all the combustion regimes in the hydrogen-air mixture are significantly shallower than for H_2/O_2. Fig.9 shows scales of the temperature gradients depending on T*, calculated for the detailed chemical model for H_2-air mixture.

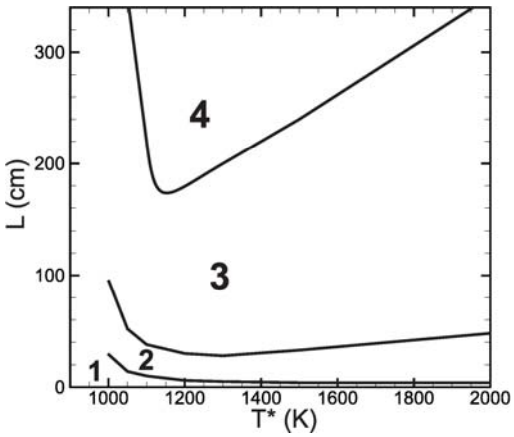

Figure 9 Scales of the temperature gradient in H_2-air corresponding to the boundaries between regimes 1, 2, 3, 4 for a detailed chemical model.

COMBUSTION REGIMES INITIATED BY TRANSIENT ENERGY DEPOSITION

In the majority of practical cases ignition arises from a small volume of combustible mixture which is locally heated by energy input by means of an electric spark (e.g. a spark-plug in an engine combustor), hot wire, focused laser light etc. Such a transient energy addition results in the formation of the initial non-uniform distribution of temperature leading to the gas expansion and initiation of different regimes of combustion depending on the amount and the rate of energy actually added. Transient thermal energy deposition into a reactive gas may be a source for ignition of either deflagration or detonation. Sufficiently fast and large energy addition can facilitate direct initiation of detonation. However the particular mechanisms of the direct initiation of detonation or initiation of deflagration can be different. Detonation can be initiated by a strong shock (strong explosion) or it can arise as a result of the formation of an appropriate temperature gradient through the Zeldovich' gradient mechanism.

We consider classification of the regimes of chemical reaction wave initiated by the transient energy deposition in gaseous mixtures using high resolution numerical simulations of reactive Navier-Stokes equations, including a multispecies transport model, the effects of viscosity, thermal conduction, molecular diffusion and a detailed chemical reaction mechanism for hydrogen-oxygen mixture [21]. Such a level of modeling allows clear understanding of the feedback between gasdynamics and chemistry which is the principal point when studying unsteady process of ignition and practically cannot be captured using a simplified gas-dynamical and chemical models.

We assume uniform initial conditions and a transient energy deposition localized on the scale of the "hot spot" $0 \le x \le L$. Combustion regime initiated by the energy deposition depends on the interrelationship between the characteristic times of the problem [21]: time of the hot spot heating Δt_Q, acoustic time $t_a = L/a(T)$, which defines the concomitant motion setup in the mixture, with the speed of sound $a(T)$, time of heat propagation, $t_T \approx L^2/\chi$, where χ is the thermal conductivity coefficient, and the ignition time t_{ign}, which characterizes length of the endothermic chain initiation stage after or during the energy deposition, $t_{ign} = t_{ind}(T,P)$. For the sake of simplicity we assume that the rate of the energy addition is linear in time, so that total energy deposition into the hot spot

is $Q_{ig} = W\Delta t_Q$, where W is the power of the external source of energy.

In case of the fast energy deposition, $\Delta t_Q << t_a$, the time scales of the hot spot heating is shorter then acoustic time. The local heat addition occurs as a nearly constant volume process and the temperature elevation within the hot spot is accompanied by a concomitant pressure rise. Subsequent expansion of the hot spot driven by the large pressure gradient causes compression and shock waves in the surrounding gas. If $\Delta t_Q < t_{ign} << t_a$, the reaction starts after the end of the energy deposition. It should be noted that depending on the value of deposited energy the mixture of the hot spot achieves some temperature and pressure at which the reaction starts and the combustion regime then develops by the volumetric explosion at these conditions. For a very short time of energy addition, much less than the acoustic time, mixture in the hot spot can be heated to any temperature and the ignition regime will be determined by the induction time at the obtained temperature and pressure. For the temperature range $T = (1100 - 1500)K$, where the exothermic reaction starts, the induction time is about ten microseconds. Therefore, if the reaction started, further heating and energy deposition do not matter and do not influence the formed combustion regime. If the power is large enough, subsequent events represent the decay of the initial discontinuity consisting of a compression wave propagating out of the hot spot, which steepens into the shock wave and the rarefaction wave propagating inside from the boundary of hot spot with the velocity equal to the local sound speed. This scenario is similar to a strong point explosion [22] and it results in the direct triggering of a detonation wave if a concomitant shock wave at the right boundary is strong enough (e.g. for L=1cm, $Q \geq 3.0 kJ/m^2$). Another possibility is a detonation initiation via the Zeldovich gradient mechanism due to the shallow gradient formed by the rarefaction wave at the increased pressures in the hot spot region. In case of the rapid but relatively small energy deposition (e.g. for L=1cm, $Q < 3.0 kJ/m^2$) the resulting regime is a fast deflagration wave with runaway shock wave. For longer energy deposition, the ignited combustion regime will depend on the size of the hot spot and correspondingly on the relation between Δt_Q and t_a. For example, if $\Delta t_Q >> t_a$ the acoustic waves have enough time for pressure equalization and the local heat addition occurs at nearly constant pressure.

Here we restrict ourselves by several examples demonstrating role of gasdynamics in the formation of different combustion regimes. First, we consider cases when the time scale of the energy deposition is comparable to or shorter than the acoustic time scale and less than the induction time at the ignition temperatures, $\Delta t_Q < t_a < t_{ign}$. Figure 10 shows the evolution of the temperature and pressure profiles inside the hot spot ($L = 1cm$) during the energy deposition. The rarefaction wave propagating to the left creates shallow temperature and pressure gradients on the scale of about the size of the hot spot. At the initial pressure P_0=1atm such temperature gradient on the scale 1cm is not enough for triggering a detonation. However, since the pressure of the heated mixture increased during the heating up to about 4atm, this temperature gradient can produce a detonation through the Zeldovich gradient mechanism. The calculated temperature and pressure profiles in Fig.10 demonstrate the emergence of the spontaneous reaction wave and its coupling with the pressure wave leading to the detonation initiation.

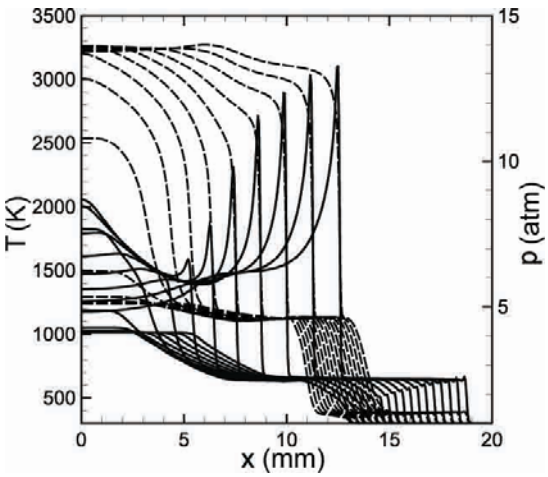

Figure 10 Evolution of temperature (dashed lines) and pressure (solid lines) profiles and a detonation formation (L=1cm, Δt_Q=5μs, Δt=0.5μs).

The rapid energy deposition such that the heating time, Δt_Q, is less or comparable to the acoustic time scale of the volume, always results in the shock waves propagating away from the hot spot. A particular scenario of the resulting combustion regime depends on the size of the hot spot, though the basic physics appears to be similar to that described above. Different possible scenarios include either direct initiation of detonation through a constant volume explosion by a strong enough shock wave in the context of a thermal explosion, or through the Zeldovich gradient mechanism due to the shallow gradient formed by the rarefaction wave at the

increased pressures in the hot spot region, or the shock waves propagating away from the hot spot producing ignition of the fast deflagration propagating behind the shock waves (regime 3 according to the classification of combustion regimes in previous section).

The scenario of thermal energy addition over a longer period of time is different. If the acoustic time is much less than the energy deposition time, $t_a << \Delta t_Q \le t_{ign}$, then there is enough time for pressure to be spatially homogenized by acoustic waves. In this case there are no strong compression waves emitted from the hot spot and the initiated combustion regimes depend essentially on the steepness of the temperature gradient, which is formed by the thermal wave and gas expansion in the vicinity of the hot spot. During the time of energy deposition the thermal wave propagates away from the hot spot at the distance $x_T \approx (\chi \Delta t_Q)^{1/2}$, and the expelled mass together with the thermal wave give rise to the temperature gradient in the surrounding mixture behind the boundary of the hot spot.

Fig. 11 shows the calculated temperature gradient formed at the end of the energy deposition. The thermal wave and the gas expansion are too slow to expand temperature considerably and to form a shallow enough temperature gradient compatible with the detonation formation at atmospheric pressure. Long before the thermal wave moves away at a sufficiently long distance the temperature of the mixture rises to ignite the reaction, so that either a deflagration or a fast deflagration wave will be formed.

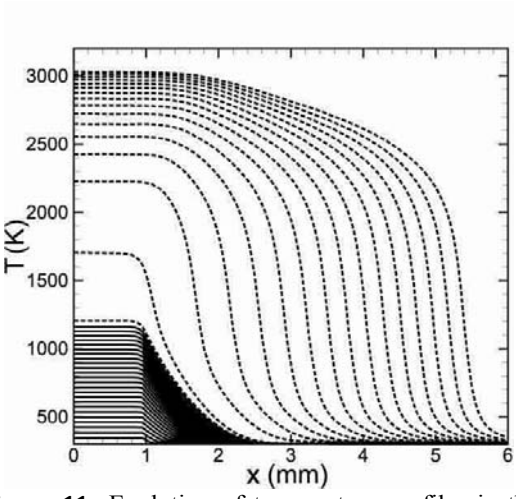

Figure 11 Evolution of temperature profiles in the hot spot (Δt=5μs) during energy deposition (solid lines) and during the deflagration wave formation (dashed lines) for L=1mm, Δt_Q=1ms, P_0=1atm.

Since the coefficient of thermal conductivity does not depend on pressure, and the steepness of the temperature gradient for direct detonation initiation through the Zeldovich gradient mechanism decreases considerably with the increase in pressure, the temperature gradient created by the thermal wave can trigger detonation at high enough initial pressure. To elucidate the process we consider a relatively small hot spot of size 1mm at initial pressure P_0= 10 atm. Figure 12(a) shows the calculated temporal evolution of temperature and pressure profiles illustrating formation of the temperature gradient outside of the hot spot, L=1mm, the development of the spontaneous wave and the transition to detonation for the energy deposition time Δt_Q=1ms.

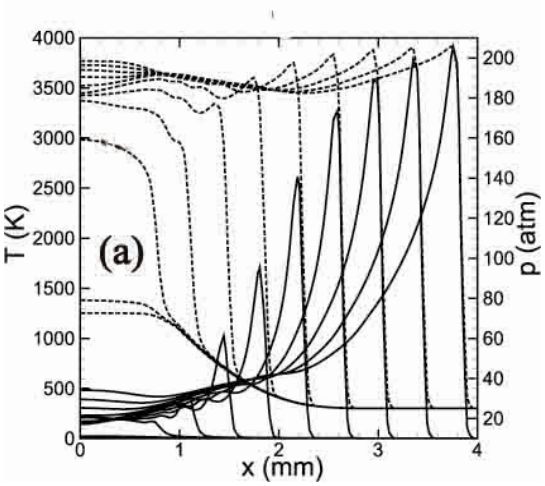

Figure 12(a) Evolution of temperature (dashed lines) and pressure (solid lines) profiles on the gradient formed in the energy release region.

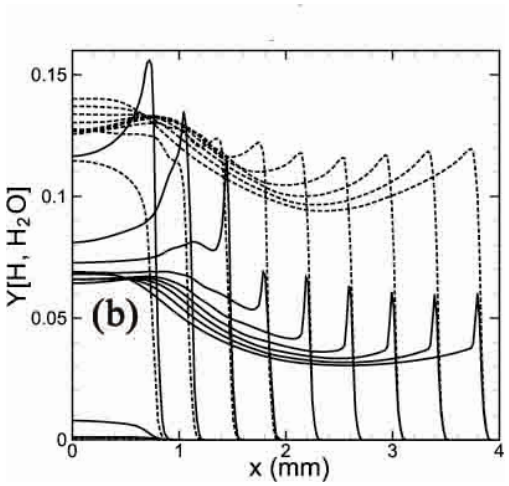

Figure 12(b) Evolution of the concentration profiles of H radicals (solid lines) and the combustion products H_2O (dashed lines) for the conditions of Fig. 12(a); Δt=0.15μs. .

Figure 12(b) shows the corresponding evolution of the concentration profiles for H radicals and the combustion products (H_2O), illustrating the development of a detonation wave.

DEFLAGRATION-TO-DETONATION TRANSITION

It is known for a long time that a flame ignited near the closed end of a tube and propagating to the open end may spontaneously accelerate until a sudden abrupt increase of the flame velocity, which ends up with triggering a detonation. The first experimental study of the transition from deflagration to detonation has been made by famous French scientists Mallard and Le Chatelier in 1883 [23]. Over the past decades significant efforts have been devoted to understanding the nature of the flame acceleration and mechanism of the transition from deflagration to detonation (DDT) because of its important applications ranging from industrial safety, nuclear power plants safety, potential application for micro-scale propulsion and power devices, and to deciphering of scenario of white dwarf thermonuclear explosion in Supernovae events. Over the years DDT was one of the least understood processes in combustion science in spite of its extreme importance. Significant insights have been obtained by a long series of experimental, theoretical and numerical studies by different groups of authors. Yet many questions still remain unresolved or poorly understood and the DDT topic is considered as one of the major challenges of combustion science.

Without a doubt one of the main difficulties for modeling and understanding the mechanism of DDT is the necessity to use a detailed chemical reaction model. Most of the theoretical and numerical works made in attempt to understand DDT used a one-step kinetics model. Different answers have been given to the principle problem regarding the mechanisms responsible for the transition to detonation, including turbulent mixing, boundary layers, hydraulic resistance, etc. A general conclusion, based on the modeling DDT using used a one-step kinetics model, was that hot spots are formed in nearby unreacted material ahead the flame that lead to detonation formation through the Zeldovich gradient mechanism ([24] and references within). However the experiments [25] and 2D and 3D simulations, which used detailed chemical reaction models [26-29], have shown that temperature in the mixture ahead of the flame front is too low to ignite reaction on the time scales of the whole process. Moreover, the spatial scale of the temperature non-uniformity in the hot spots is at least by the order of magnitude smaller than that capable to ignite detonation via the Zeldovich gradient mechanism.

Flame Acceleration in Tube with Non-slip Walls

From the very beginning of DDT studies the very fact of the flame acceleration in tubes has been considered as an important factor that influences the DDT process. The flame acceleration and the transition to detonation have been studied using the one-dimensional and multi-dimensional analyses taking into account that the acceleration rate can be enhanced by external turbulence or intrinsic flame instabilities. The classical formulation of the problem in question and an experimental set-up is an initially laminar flame ignited near the closed end and propagating to an open end of the tube. The accelerating flame acts like a piston pushing into the flow ahead of the flame compression waves, which are steepening into the shock waves. From the earlier studies a common belief was that the crucial aspect for DDT and the fast flame acceleration is possible only for a strongly turbulent flames. The experiments demonstrated that the presence of obstacles along the channel walls increases the flame acceleration toward the open end if the flame passes through an array of turbulence-generating baffles and the presence of obstacles shortens considerably the run-up distance. This presumably was the reason why the first attempts to explain DDT were associated with turbulent flames and were based on assumption that DDT might occur only in the case of turbulent flames. Channels with rough walls or obstacles are often used to study DDT since in this case the run-up distance is more or less controlled. All the same DDT occurs in channels with smooth walls and even in thin capillary tubes where the flow is a laminar one. The experimental flame velocity-time dependence during DDT in a channel with smooth walls is shown in Fig.13 [25].

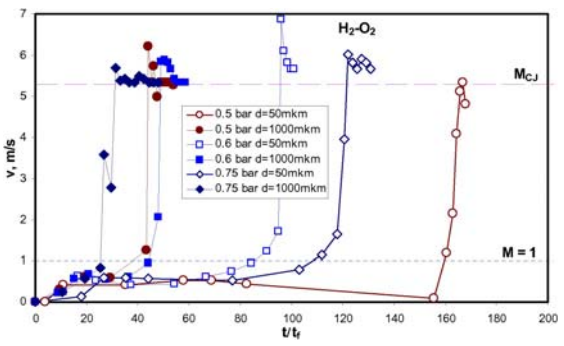

Figure 13 Flame dynamics during the detonation initiation. Flame velocity is in units $M=U_f/a_{s0}$.

From the very beginning of the DDT research Ya. B. Zeldovich pointed out that the transition to detonation requires the formation of a strong shock wave, and therefore it is necessary that the flame propagates with the acceleration. Explaining the nature of the flame acceleration in the DDT events he also questioned the idea about turbulence as the main reason of the flame acceleration, pointing that turbulence is not a primary factor responsible for flame acceleration in a smooth-walled channel and sequential detonation formation, but that the flame accelerates primarily due to stretching of the flame surface caused by a non-uniform velocity profile in the flow ahead of the flame.

To elucidate mechanism of a flame acceleration and DDT we shall not consider the ignition and the early stage of a finger flame acceleration, but we consider a flame, which is initiated as a planar one near the closed end and propagates to the open end of a tube with non-slip walls. At the beginning, expansion of the combustion products causes the flow ahead of the flame with the longitudinal velocity, $u = (\Theta\text{-}1)U_f$, which drops to zero at the tube walls within the boundary layer. Here $\Theta = \rho_u / \rho_b$ is the density ratio of the unburned ρ_u and burned ρ_b gases, respectively, and U_f is the normal flame velocity relative to the unburned fuel. The upstream flow in a channel acquires a non-uniform velocity profile due to the non-slip boundary conditions at the wall. For smooth non-slip walls the upstream flow remains almost uniform in the bulk of the channel with the longitudinal flow velocity, which drops to zero within a thin boundary layer. The velocity profile for a steady motion in a tube with non-slip walls is the Poiseuille flow with parabolic velocity profile. However, for a non-stationary flow a certain time is required for establishing the Poiseuille parabolic velocity profile. The time needed for the development of the Poiseuille parabolic velocity profile in the flow ahead of the flame can be estimated using the Blasius solution for the boundary layer (H. Blasius, L. Prandtl) and taking into account that the Poiseuille flow is established when thickness of the boundary layer became of the order of the channel width [26]. For a laminar boundary layer of thickness $\delta \approx 2.95\sqrt{L\nu / u} \approx L / \sqrt{Re}$, where L is the characteristic length of the flow, and Re is the Reynolds number, we obtain time, which is required for establishing the Poiseuille flow: $t_P \approx D^2 / 36\nu$. This time is much longer than duration of the whole process for typical experimental conditions. For example, $t_P \approx 2\,s$ for the channel of width 5cm, while duration of the whole process is about 1 ms.

Thus, the flow and the average velocity ahead of the flame remain nearly uniform in the bulk. Since the flame velocity at each point of the flame front is the sum of the normal flame velocity relative to the moving gas ahead and the velocity of the flow ahead of the flame, the shape of the flame front reproduces according to Huygen's principle the velocity profile in the upstream flow. The flame skirt is stretched backward within the boundary layer, which results in the increase of the flame front surface and, correspondingly, in the increase of the burning rate, which is proportional to the relative increase of the flame surface. With accuracy $\delta / D << 1$, the flame velocity can be written as

$$U_{fL} = \Theta U_f \cdot \exp\{\alpha U_f t / D\}, \qquad (12)$$

where α is numerical factor of the order of unity. The accelerating flame acts as a piston producing compression waves in the flow ahead. The time and the coordinate, where the compression wave steepens into a shock wave are determined by the condition that the Riemann solution for a compression wave becomes a multi-valued function. During the stage of the exponential increase of the flame velocity, the shock waves are formed at $x = X_{sh}$ far ahead of the flame front (located at $x = X_f$) at the distance about $L=X_{sh}-X_f \approx (5\div7)D$ from the flame front [26].

Since flow ahead of the flame can be viewed as one formed behind the leading shock, we can estimate the thickness of the laminar boundary layer $\delta \approx (X_{sh} - X_f) / \sqrt{Re}$, where $Re = (\Theta - 1)U_f D / \nu$ is the Reynolds number in the upstream flow. Theoretical estimate for the boundary layer thickness gives $\delta \approx (0.3 \div 0.4)\,mm$. From the numerical calculations [26-29] the boundary layer thickness was found about 0.4mm for D=10mm. For a wide channel the Poiseuille flow ahead of the flame is not formed till the transition to detonation and the condition $\delta / D << 1$ holds.

We can also find the width of a channel for which the Poiseuille flow is established almost from the very beginning. The channel must be so narrow that thickness of the boundary layer is of the order of the channel width. Taking into account that the flow ahead of the flame is produced by the leading shock, this leads to an estimate $5D / \sqrt{Re} \approx D$, or $Re \approx 25$. It is convenient to express the Reynolds number in terms of the flame thickness L_f and the normal velocity of a laminar flame $Re \approx \Theta D / L_f$, taking into account $L_f U_f \simeq \nu$ (see e.g. [16]). Taking for hydrogen-oxygen at 1atm $L_f = 0.24\,mm$, $U_f \simeq 10\,m/s$, $\Theta \approx 8.3$, we find that the Poiseuille

flow is established for the width of the channel smaller than $D_{cr} = 25L_f / \Theta \approx 1\text{mm}$. For the ethylene/oxygen flame at 1atm, $L_f = 0.075\text{mm}$, $U_f = 5.5\text{m/s}$, $\Theta = 14$ and the critical width of the channel is about 0.35-0.4mm, which is in a good agreement with the DDT experiments in microscale tubes.

As the edges of the flame front are stretched along the wall within a boundary layer, a narrow fold is formed within the boundary layer between the edge of the flame front skirt and the wall. As the fold becomes deeper and the angle at the fold's tip became smaller, some part of the flame front near the fold's tip, approaching the wall, is quenched due to the heat loss at the wall. Simple geometric consideration [26] shows that the corresponding time of the flame skirts quenching is $t_2 \approx D\delta / 2\Theta L_f U_f$. Partial quenching of the flame front results in reducing of the total flame surface and therefore decreasing the rate of the flame acceleration. Since $t_2 \approx D\delta / 2\Theta L_f U_f$ is much smaller compared to the characteristic time of the flame acceleration D / U_f ($\delta / L_f 2\Theta << 1$) the flame acceleration (12) is constant with accuracy of the first order terms of series expansion in $\delta / L_f 2\Theta << 1$. Therefore, during the next stage, $t > t_2$, the flame velocity-time dependence can be approximated as

$$U_{fL} \simeq \Theta U_f \left[1 + \beta (t / \tau_f)^n\right], \quad 0 < n < 1 \qquad (13)$$

Specific value of the exponent n in (13) does not matter since we are interested only in the location where the shock wave is formed. It can be shown [26] that for a piston moving with the velocity-time dependence (13) the Riemann solution for a simple travelling wave is multi-valued everywhere for any values of 0<n<1. Therefore, during the stage, $t > t_2$, the compression wave produced by the flame steepens into the shock directly on the surface of the flame front.

Contrary to a stationary flame, the flow with the accelerating flame is not isobaric. In the latter case pressure is growing at about the same rate as the flame velocity. From the time when the compression waves steepen into the shock close to the flame front, the unreacted mixture of considerably higher density compressed and heated in the shock starts entering the flame front and produces a narrow pressure peak on the scale of the flame front width. While during the first stage the flame acceleration is due to the stretching of the flame front within a boundary layer, during the second stage subsequent acceleration of the flame is due to its coupling with the shock wave formed at the flame front. Consequently, there are two feedback mechanisms leading to the increase of the flame speed. One is driven by the increased temperature, and hence reactivity, of the mixture due to the shock, and the other by the increased density and hence amount of reacting fuel entering the flame front. A higher flame speed causes a higher gas velocity ahead of the flame. After the flame was accelerated up to the local sound speed the shocks and the pressure peaks do not run away from the reaction zone, where they were formed, and the pressure peak is localized directly in the reaction zone. Consequently, the amplitude of the pressure peaks at the flame front continues growing due to the combustion of larger amount of unburned mixture entering the reaction zone during this stage. Eventually, the pressure peak becomes strong enough to affect the reaction rate. The increase of pressure enhances reaction rate and the increased heat release in the reaction zone creates a positive feedback coupling between the pressure pulse and the heat released in the reaction. It results in more violent increase of the pressure peak, which finally steepens into the shock strong enough for formation of a detonation wave. Duration of the last stage of actual transition to detonation, when the pressure peak steepens into the shock, is defined by the condition of intersection of characteristics leaving the top and the pedestal of the pressure pulse: $L_f / a_s \approx 6\mu\text{s}$, which is consistent with the results of numerical simulations.

Numerical Simulations of Flame Acceleration and Deflagration-to-Detonation Transition

Direct numerical simulations of the flame propagating in channels with non-slip walls filled with the stoichiometric hydrogen-oxygen mixture at initial temperature T_0=298K and initial pressure P_0=1atm were performed for 2D channels of different widths from 1mm to 10mm [26-28] and for 3D rectangular channel with cress section 10⊗10mm [29] with the minimum computational cell size $\Delta = 0.005\,\text{mm}$, which ensure high resolution of the flame front, which width is 0.25mm, and convergence of the solutions. A laminar planar flame was initiated near the left closed end and propagates to the right open end of the channel. The computations solved the multidimensional, time-dependent, reactive Navier-Stokes equations including the effects of compressible gas convection, molecular diffusion, thermal conduction, viscosity and different detailed chemical kinetics schemes for the reactive species H_2, O_2, H, O, OH, H_2O, H_2O_2, and HO_2.

The grid system for the 3D modeling of DDT was built out from 50 million up to 400 million grid

points, which resolves flame front using at least 12 computational cells. The overall dynamics in 2D and 3D cases is similar except the higher acceleration rate associated with additional degree of freedom in case of 3D channel.

Figure 14 shows the overall picture of the 3D flow, the flame front evolution and the transition to detonation. Cross sections of the 3D images in the plane (x, y, z=5mm) and the streamlines are shown at the right part of Fig. 14. To analyze the influence of flame surface topology, the additional small perturbations were imposed in the beginning of the flame propagation. They cause formation of the flame brush, which shortly develops in many well pronounced bulged tips. The compression waves produced by the accelerating flame are seen as slightly corrugated surfaces ahead the flame front. They steepened into the shock waves far ahead of the flame not shown in the frames.

It is seen that the flow ahead of the flame remains almost uniform in the bulk of the channel. The boundary layer is seen as lighter white strip on the bottom and back walls of the channel. It should be emphasized that the 2D images representing by the cross sections in the plane (x, y) do not resemble the experimental schlieren photographs, but rather similar to those obtained in 2D simulations. The shape of the flame propagating in the channel depends on the small perturbations imposed in the beginning of the process.

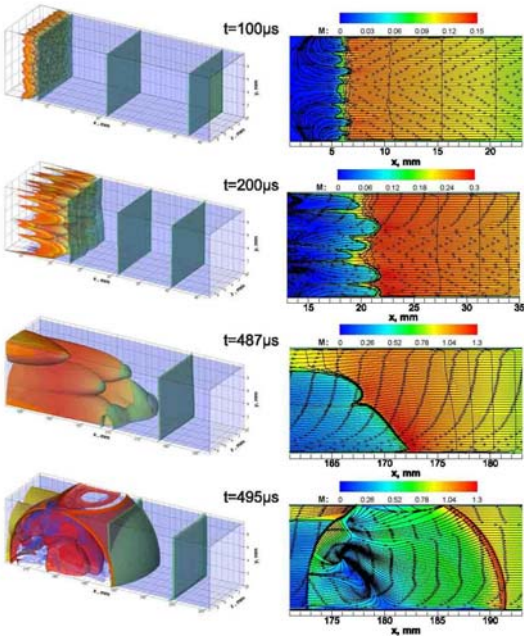

Figure 14 The flame structure and compression (shock) waves (green surfaces) at sequential times 100, 200, 487 and 495μs (left) and the corresponding 2D cross sections of 3D images in the plane (x, y, z=5mm) at the right part.

While in 2D case the main direction of the flame propagation is associated with the side walls, and initially planar flame evolves into the tulip-shaped or single mode flame, which leading tips are moving along the walls, in 3D case the edges between the channel walls are a preferential orientation for the flame propagation.

Shortly before the transition to detonation the shock waves are formed close to the leading bulged tip of the flame and practically "sits" at the flame tip (frame t=487μs). Then, after 8μs the flame turns in a detonation wave. The pre-detonation time estimated as time when the pressure reaches its maximum, and when the strong shock arises on the flame tip, overcomes the sonic barrier and forms a detonation behind its front, is 0.55 ms for the 3D channel and 1.35ms for the 2D channel. It should be noted also, that temperature ahead of the flame front does not exceed 500-600 K all the time till the moment of the actual transition to detonation, so that the rates of chemical reactions ahead of the flame are negligibly small, and temperature non-uniformities if any ahead of the flame can not produce a detonation through the Zeldovich gradient mechanism.

The temporal evolution of the flame speed and the pressure peak at the leading flame tip throughout the process of the flame acceleration and DDT computed for 3D channel is shown in Fig. 15.

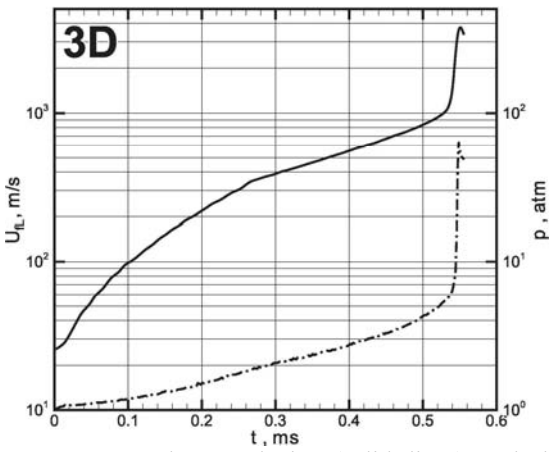

Figure 15 Flame velocity (solid lines) and the pressure peak (dash-dotted lines) time dependences computed for 3D channel.

Figure 16 shows zoomed picture of the temporal evolution of the combustion wave velocity during the initial stage computed for 3D and 2D channels of the same width D=10mm. The exponential increase of

the flame velocities for the first stage is shown by dashed lines, while velocity-time dependence on the next stage can be approximated by the expression (13).

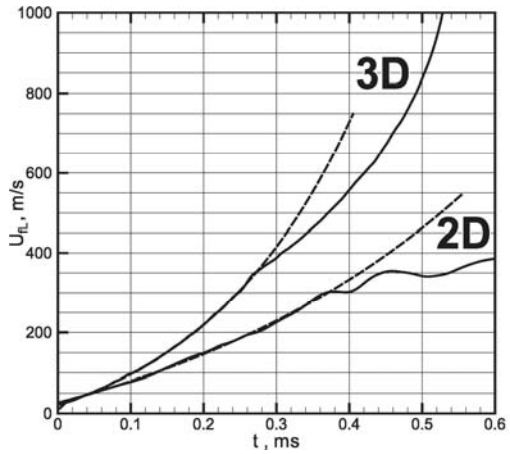

Figure 16 The initial stage computed for 3D and 2D channels of the same width D=10mm.

The computations confirmed the theoretical prediction that after the end of the exponential stage of flame acceleration, a larger amount of the fresh fuel starts entering the flame front, which results in the development of a narrow pressure peak on the scale of the flame width shown in Fig. 17. Consequently, the amplitude of the pressure peaks at the flame front continues growing due to the combustion of larger amount of compressed mixture entering the reaction zone during this stage.

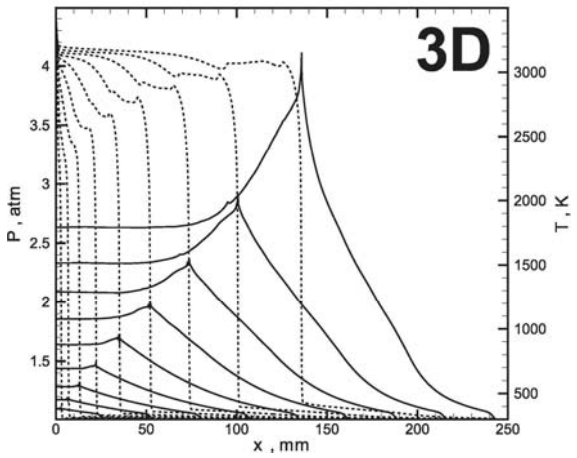

Figure 17 Temperature (dashed lines) and pressure (solid lines) profiles corresponding to leading point of the flame front represent the flame structure and the pressure peak formation from t_0=50μs, Δt=50μs, t_f=500μs.

Formation of the pressure pulse and the mechanism of transition to detonation shown in Fig. 17 for 3D case is similar in both 2D and 3D cases. For both 2D and 3D cases the velocity-time dependence plots demonstrate the same feature of several distinctive stages of the flame acceleration: initial stage of flame expansion out from the ignition zone; the stage of exponential increase of the flame velocity; the stage when the rate of the flame acceleration decreases compared with the previous exponential stage; the final stage of sharp increase of the flame velocity and actual transition to detonation. For 3D case the run-up distance and duration of the flame propagating before the transition to detonation are about three times shorter compared to 2D channel of the same width. The pre-detonation time estimated as time when the pressure reaches its maximum, and when the strong shock arises on the flame tip, overcomes the sonic barrier and forms a detonation behind its front, is 0.55 ms for the 3D channel and 1.35ms for the 2D channel. All the same, temperature ahead of the flame front does not exceed 500-600 K all the time till the moment of the actual transition to detonation, so that the rates of chemical reactions ahead of the flame are negligibly small, and temperature non-uniformities if any ahead of the flame can not produce a detonation through the Zeldovich gradient mechanism.

DDT Experiments and Its Interpretation

To capture the features of flame acceleration and the origins of detonation one needs accurately resolve both time and space scales, which are far beyond the limits of the nowadays temporary resolution of the cameras used in DDT experiments. In most cases one can recognize moment of DDT using only two sequential snapshots. The first one shows the flow pattern in the vicinity of the flame front, and the second one shows already the detonation wave propagating at the background of the previous flow pattern. The highest time resolution of 5μs was achieved in high-resolution stroboscopic Schlieren photographs by Urtiew and Oppenheim [30]. The photographs were taken with a light source consisting of a ruby laser with a short pulse width (10^{-8} s) and high repetition rate (up to 106 frames per second). The photographs show the initiation of a detonation from a "local explosion" within the shock–flame complex, the so-called ''explosion in the explosion.''

On the contrary, with nowadays computers development the available time and space resolution of the process is much higher than that can be obtained experimentally with schlieren method. It became much more feasible and can bring much better understanding about the DDT origin. Besides,

3D computer simulations provide us with three-dimensional images of the process not available with the schlieren technique, which in any case provides us with only 2D projection of the three dimensional flow, until holographic photos are not available for combustion experimental technique.

As an example, Figure 18 shows sequence of the computed shadow photographs in the cross section XY of the flow and the flame during the first stage of flame acceleration presented in Fig. 14 at 200μs and 300μs: the frames (a) and (b), correspondingly. The frame (c) in Fig. 18 is shadow photograph obtained experimentally [25] for the initial stage of the flame acceleration. One can see that the flame in the photos looks like a turbulent one, which is usually named "turbulent flame brush". However, it is seen from the 3D images in Fig.14 that either flame or flow are not turbulent. The "turbulent" pattern here is a result of interference of light beams refracted on the different pieces of cellular flame surface. This issue shows that the cellular laminar flame can be visualized and interpreted as a turbulent one on the images giving 2D projections of the 3D flow and may cause misinterpretation of the studying phenomena. Similar misinterpretation may cause shadow visualization of the flow on the second stage.

Figure 19 shows computed shadow photos, corresponding to the beginning of the second stage at time 487μs in 3D image of Fig. 14 in two projections: the XY cross section (a) and the XZ cross section (b).

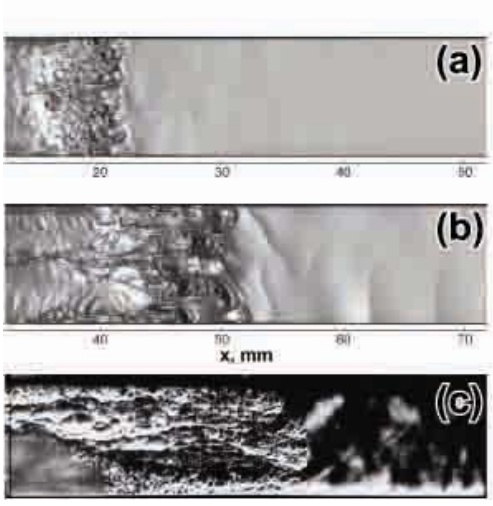

Figure 18 Computed shadow photos of the flow and flame for the first exponential stage of the flame acceleration at (a) 200 ms and (b) 300 ms, correspondingly); (c) is the experimental shadow photos at the same stage.

The frame (c) in Fig. 19 is the experimental shadow photo [25]. Both images look like "turbulent flame brush". However they are different and structure of the frame (b) for the XZ cross section is more similar to the experimental shadow photo on the frame (c).

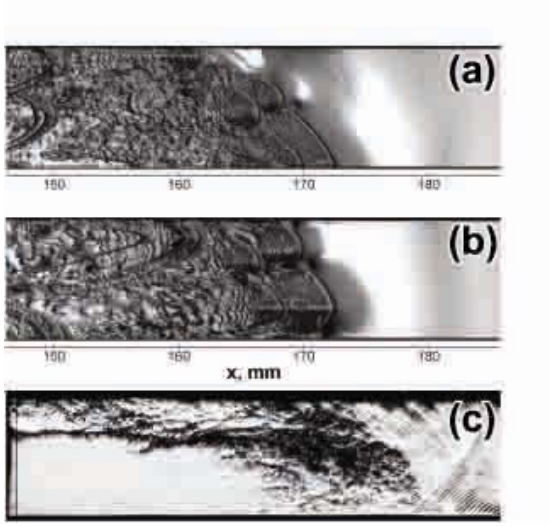

Figure 19. Computational shadow photos in the XY (a) and XZ (b) cross sections at t=487μs; (c) – experiment [26].

Fig. 14 shows that at the moment of detonation formation the flame surface is multidimensional. It consists of several bulge tips that are advanced far ahead compare with neighboring flame bulges. These bulge tips represent leading tips of the flame front, where the pressure pulses arise. On the contrary the shadow photos show projection of all planes intersecting the flame surface along the side wall of the channel. In the diagnostics plane one can observe the flame position and the shocks intersection points ahead of it, which can be different depending on what cross section XY or XZ planes was chosen for the shadow visualization (See Fig. 19). These intersection points produce the signals coming to the diagnostics plane out from the density gradients on the shock fronts radiated by the leading flame edges. Note, that the detonation is formed in the reaction zone on the flame edge according to the mechanism described above. There are no proper conditions in the intersection points to ignite detonation via local autoignition of the mixture. However, since the part of the flow including the leading flame edge can be clouded by the laser knife used in schlieren visualization, the planar projection may show the detonation arising ahead the flame front. In this case it looks at the shadow photos as if detonation wave is formed ahead the flame front as it is shown in Fig.20.

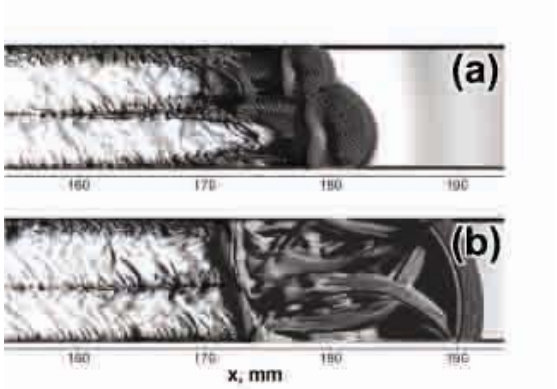

Figure 20. Computed Schlieren visualization of the flow in the XZ cross section after DDT: (a) 492μs; (b) 495μs.

In fact, it is seen from 3D images in Fig. 14 that the phenomenon, which is often quoted as "explosion in the explosion", does not originate out from the "hot spot" formation in the heated fuel-air mixture. It could be viewed as an artifact of the diagnostics caused by the lag between the leading edge of the flame where detonation arises and the remaining flame surface. Depending on how the schlieren or shadow photos were taken, the obtained image and interpretation of the one and the same phenomenon can be quite different which can lead to misinterpretation of underlying physics. One can observe such a case comparing shadow photo in Fig. 20(a) and Fig. 21(b), where Fig. 21 shows computed shadow photos for the last stage of the transition to detonation. The frames (a), (b), (c) in Fig. 21 correspond to 487μs, 492μs and 495μs of Fig.14 and show the detonation formation. The frames (d, e) in Fig.21 represent the same phase of the process obtained in experimental shadow photos [25] with the time resolution $\Delta t = 100\mu s$. The frame (d) corresponds to the frame (a), while the frame (e) shows already developed detonation corresponding to the frame (c). In the experimental shadow photos the information about how the flame was transformed into the detonation is lost. On the other hand a good qualitative similarity of the computed shadow photos of flow patterns and the experimental photos confirms that the simulations reproduces correctly the observed process.

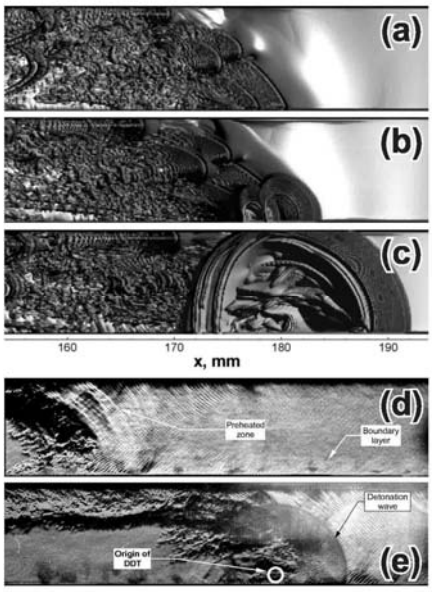

Figure 21. Computational shadow photos for the last stage of DDT at: a) 487μs, b) 492μs, c) 495μs. Frames d) and e) are the experimental shadow photos with time resolution Δt=100μs [25].

CONCLUSION

This lecture aimed to communicate two messages regarding fundamentals of unsteady combustion processes. First, it should be noted that the understanding of combustion phenomena related to unsteady processes obtained on the basis of a one-step chemical model can be incorrect even qualitatively and therefore may require revision on the basis of a detailed chemical model. The second is the complex nature of chemical reaction mechanisms and its response to the various pressure-dependent chain mechanisms. Consequently, combustion modeling using a reduced reaction mechanism should be conducted with caution, especially in the case of unsteady processes when wide variations in pressure, temperature, and composition are embedded in the phenomena under study. It is further noted that although the illustrations presented herein were based on hydrogen-oxygen, the same concepts carry over to hydrocarbon oxidation because their mechanisms are similarly affected by chain reactions, and because they must necessarily contain the hydrogen oxidation as a key component. Finally, it should be noted that though the difference in induction time given by different chemical schemes at the low temperature region has little effect on the calculated flame speed at the normal or low pressures, it is not the case at high pressures, when three body collisions become

important and the induction time is shifted to lower temperatures. More reliable schemes are those which give closer value of the induction time to the experimentally measured at low temperatures.

Acknowledgment

The computations were performed on resources provided by the Swedish National Infrastructure for Computing (SNIC) at the Center for Parallel Computers at the Royal Institute of Technology in Stockholm and the National Supercomputer Centers in Linkoping. The author is grateful to A. Kiverin, A. Smygalina, M. Ivanov and I. Yakovenko for many fruitful discussions.

REFERENCES

[1] Maas U., Warnatz J., Ignition Processes in Hydrogen-Oxygen Mixture, *Combust. Flame*, Vol.74, 1988, pp. 53-69.

[2] Sloane T.M., Ronney P.D., A Comparison of Ignition Phenomena Modeled with Detailed and Simplified Kinetics, *Combust. Sci. and Tech.*, Vol. 88, 1993, pp.1-13.

[3] Konnov AA. Remaining uncertainties in the kinetic mechanism of hydrogen combustion, *Combust Flame*, Vol. 152, 2008, pp. 507-28.

[4] O'Conaire M., Curran H.J., Simmie J. M., Pitz W.J., Westbrook C. K., A comprehensive modeling study of hydrogen oxidation, *Int. Journal of Chemical Kinetics*, Vol. 36, 2004, pp. 603-622.

[5] Konnov A.A. Refinement of the Kinetic Mechanism of Hydrogen Combustion, *Khimicheskaya Fizika* , Vol. 23, 2004, pp.5-18.

[6] Warnatz J., Maas U., Dibble R.W., Combustion. *Physical and chemical fundamentals, modeling and simulations, experiments, pollutant formation*, Springer-Verlag, Berlin, Germany, 2006.

[7] Kusharin A.Y., Agafonov G.L., Popov O.E., Gelfand B.E., Detonability of $H_2/CO/C0_2$/Air Mixtures, *Combust. Sci. and Tech.*, Vol. 135, 1998, pp.1-6.

[8] Kusharin A.Y., Popov O.E., Agafonov G.L., Burning velocities of oxygen-hydrogen mixtures with steam, *Chem. Phys. Rep*. Vol. 14, 1995, pp. 584–594.

[9] Smith G.P., Golden D.M., Frenklach M, Moriarty N.W., Eiteneer B., Goldenberg M., et al. *Gri-mech 3.0*, <http://www.me.berkeley.edu/grimech>; 2002.

[10] Hirschfelder J. O., Curtiss C. F., Bird R. B., *Molecular theory of gases and liquids*, Wiley, New York, 1964.

[11] Hairer E, Wanner G. Solving ordinary differential equations. Stiff and differential-algebraic problems. New York, Springer-Verlag; 1996.

[12] Belotserkovsky O.M., Davydov Yu.M.: Coarse-particle method in hydrodynamics (in Russian) Publ. Inc. Nauka, Mir, Moscow, 1982.

[13] Liberman M.A., Ivanov M.F., Valuev D.M., Eriksson L.-E., Numerical modeling of knocking onset and hot spot formation by propagating flame in SI engines, *Combust. Sci. and Tech.*, Vol. 178, 2006, pp. 1613–1647.

[14] Zeldovich Y.B., Barenblatt G.I., Librovich V.B., Makhviladze G.M., The Mathematical Theory of Combustion and Explosion, Plenum, New York, 1985.

[15] Hu E., Huang Z., He J., Miao H., Experimental and numerical study on laminar burning velocities and flame instabilities of hydrogen–air mixtures at elevated pressures and temperatures, *Int. Journal of Hydrogen Energy*, Vol. 34, 2009, pp. 8741-8755.

[16] F.N. Egolfopoulos, C.K. Law, An experimental and computational study of the burning rates of ultra-lean to moderately-rich $H_2/O_2/N_2$ laminar flames with pressure variations, *Proc. Combust. Inst*. Vol. 23, 1991, pp. 333–340.

[17] Zel'dovich, Ya. B., Regime classification of an exothermic reaction with nonuniform initial conditions, *Combust. Flame*, Vol. 39, 1980, pp. 211-226.

[18] Zel'dovich, Ya. B., Librovich, V.B., Makhviladze, G.M, and Sivashinsky, G.I., On the development of detonation in a non-uniformly preheated gas, *Astronautica Acta*, Vol. 15, 1970, 313-321.

[19] Liberman M. A., Kiverin A. D., Ivanov M. F., On Detonation Initiation by a Temperature Gradient for a Detailed Chemical Reaction Models, *Phys. Letters*, Vol. A 375, 2011, pp. 1803-1808.

[20] Liberman M.A., Kiverin A.D., Ivanov M.F., Regimes of chemical reaction waves initiated by nonuniform initial conditions for detailed chemical reaction models, *Phys. Rev*. E. Vol. 85, 2012, pp. 056312(1-16).

[21] Kiverin A.D., Kassoy D.R., Ivanov M.F., Liberman M.A., Mechanisms of Ignition by Transient Energy Deposition: Regimes of Combustion Waves Propagation, *Phys. Rev*. E. Vol. 87, 2013 pp. 033015(1-10).

[22] Zeldovich Ya. B. and Raizer Yu. P., Physics of Shock waves and High-Temperature Hydrodynamic Phenonema, Academic Press, New-York-London, 1966.

[23] Mallard E, Le Chatelier H. Recherches Experimentales et Theoriques sur la Combustion des Melanges Gaseoux Explosifs. *Ann Mines*, Vol. 8(4), 1883, 274–568.

[24] Oran E.S., Gamezo V.N., Origins of the deflagration-to-detonation transition in gas-phase combustion, *Combustion and Flame*, Vol. 148, 2007, pp. 4–47.
[25] M. Kuznetsov, M. Liberman, I. Matsukov, Experimental study of the preheat zone formation and deflagration-to-detonation transition, *Combust. Sci. Technol*., Vol. 182, 2010, pp. 1628-1644.
[26] Liberman M.A., Ivanov M.F., Kiverin A.D., Kuznetsov M.S., Chukalovsky A.A., Rakhimova T.V., Deflagration-to-detonation transition in highly reactive combustible mixtures, *Acta Astronautica*, Vol. 67, 2010, pp. 688-701.
[27] Ivanov M.F., Kiverin A.D., Liberman M.A., Hydrogen-oxygen flame acceleration and transition to detonation in channels with no-slip walls for a detailed chemical reaction model, *Phys. Rev*. E, Vol. 83, 2011, pp. 056313-16.
[28] Ivanov M.F., Kiverin A.D., Liberman M.A., Flame Acceleration and Deflagration-to-Detonation Transition in Stoichiometric Hydrogen/Oxygen in Tubes of Different Diameters, *Int. J. Hydrogen Energy*, Vol. 36, 2011, pp. 7714-7728.
[29] Ivanov M.F., Kiverin A.D., Yakovenko I.S., Liberman M.A., Hydrogen-oxygen flame acceleration and deflagration-to-detonation transition in three-dimensional rectangular channels with no-slip walls, *Int. J. Hydrogen Energy*, Vol. 38, 2013, pp. 16427-16440.
[30] Urtiew P.A, Oppenheim A.K. Experimental observation of the transition to detonation in an explosive gas. Proc of Roy Soc A, Vol. 295, 1966, 13-28.